Experimental Testing of Elastic Properties of Paper and WoodEpox® in Honeycomb Panels

Krzysztof Peliński* and Jerzy Smardzewski

The literature lacks comparisons of analytical and numerical calculations that have been verified experimentally for elastic constants of auxetic cells in cores manufactured from wood materials. The aim of this study was to determine the effect of auxetic cell geometry and the type of material used in their manufacture on elastic properties of the honeycomb panel core. This paper describes properties of the materials, from which core cells were modeled and presents mathematical models of cell properties. The method of numerical optimization of cell shape was specified, and the numerical calculations concerning modeled cells are given along with the course and results of experimental tests. Additionally, the results of analytical, numerical, and experimental tests were compared. Cell geometry had a considerable effect on elastic properties of honeycomb panel cores, particularly the angle of the cell wall. Moreover, geometric imperfections had a significant effect on the results of analytical calculations. Based on numerical calculations, satisfactory consistency between these results and experimental tests was obtained.

Keywords: Auxetic; Periodic core structures; WoodEpox®; Experiment; FEM

*Contact information: Department of Furniture Design, Faculty of Wood Technology, Poznan University of Life Sciences, Poznan, Poland; *Corresponding author: pelinski@up.poznan.pl*

INTRODUCTION

Composite layered panels have been applied in the automotive, boatbuilding, military, and aeronautics industries (Gay *et al.* 2003; Pan *et al.* 2008). Honeycomb panel cores are being improved in terms of their geometry and the type of materials used. Typically they have the matrix molds composed of hexagonal, pyramidal, grid, or egg-box cells (Wadley *et al.* 2003). They are commonly manufactured from aluminum, titanium, stainless steel (Paik *et al.* 1999; Xue and Hutchinson 2006; Dharmasena *et al.* 2008; Wadley *et al.* 2013), and plastics (Herup and Palazotto 1998; Nilsson and Nilsson 2002). The cores made from metal alloys can be strengthened by adding glass fibers and carbon fibers reinforced with plastics (Rejab and Cantwell 2013). Novel solutions are connected with cores exhibiting auxetic properties and characterized by a negative Poisson's ratio. They may be applied specifically in light engineering structures (Wang *et al.* 2018). Imbalzano *et al.* (2017, 2018) examined the auxetic character of honeycomb core and found interesting behavior of auxetics at dynamic loading. The cores effectively adjusted strains by gradually condensing the material in the loaded zone. In this manner, they increased impact strength (Wang *et al.* 2014). In contrast, cores with the honeycomb structure with hexagonal cells undergo plastic deformations with no local improvement of rigidity. Wu *et al.* (2017) indicated trends in the development of layered composites in order to avoid defects resulting from the non-solid structure of the core. Yang *et al.* (2015) analytically modeled auxetic structures; however, they did not obtain any satisfactory correlation between theoretical calculations and experimental tests. Significant results of investigations concerning shape modifications of honeycomb core structures were recorded by Majewski and Smardzewski (2014, 2015). Those authors focused on the analytical modeling of delta-shaped auxetic core. At the same time, they indicated the need to further search for optimal shapes of comparable relative density. There are very few studies on applications of auxetic structures in wood-based boards. Smardzewski (2013) designed and described mechanical properties of a three-layer honeycomb panel with the auxetic core composed of bow-tie shaped cells; the auxetic core enhances strength and stiffness of furniture panels. Moreover, it facilitates substitution of particleboards and plywood traditionally used in the furniture industry with thus designed panels. In order to simplify computations for large-sized structures composed of honeycomb panels, the current trend is related with their homogenization (Guedes and Kikuchi 1990; Hohe and Becker 2001; Hartung *et al.* 2003; Geers *et al.* 2010; Park *et al.* 2016; Jeong *et al.* 2019). With homogenization of elastic properties in layered boards, the respective models are simplified, and the time-intensity of computations is reduced. However, the literature lacks comparisons of analytical and numerical calculations that have been verified experimentally for elastic constants of auxetic cells in cores manufactured from wood materials. Previous studies on the subject used only analytical and numerical models with idealized geometry (Masters and Evans 1996; Pozniak and Wojciechowski 2014; Yang *et al.* 2015; Mousanezhad *et al.* 2016; Wang *et al.* 2017). Thus, imperfections of cell shape may affect the quality of computational results. The analyses presented herein verified the hypothesis that geometric imperfections have a considerable effect on changes in values of elastic constants calculated analytically or numerically in relation to idealized models.

This study determined the effect of the geometry of auxetic cells and the type of material used in their manufacture on elastic properties of cores for honeycomb panels. Moreover, the analytical and numerical calculations for Young's moduli and Poisson's ratios were compared with results of experimental tests. First, the properties of materials used to model the core cells were described. The mathematical models describing cell properties and the numerical optimisation of cell shape were presented. After determining the numerical computations for the modeled cells, the results of analytical, numerical and experimental analyses were compared.

EXPERIMENTAL

Materials

Tests were conducted using Testliner 2 paper of 0.15 mm in thickness and grammage of 123 g/m^2 manufactured by HM Technology (Brzozowo, Poland). Moreover, WoodEpox® Abatron wood-based composite, density: 430 kg/m^3 (Abatron, Kenosha, USA) was also used. According to the manufacturer it is a wood-based material; its composition is entirely based on natural resins (zero VOC emissions and Greenguard® certificate). Elastic properties of paper, including Young's moduli MOE_x and MOE_y, moduli of rupture MOR_x (MPa) and MOR_y (MPa) as well as Poisson's ratios, ϑ_{yx} and ϑ_{xy}, for the machine direction (Y) and the cross-machine direction (X) were determined following the requirements of PN-EN ISO 1924-2 (2010). Tests were conducted on 10 strips of paper of 15 mm in width, from the original length of 180 mm. In order to determine Young's modulus, MOE_y (MPa) and MOR_y (MPa) in WoodEpox®, tests were conducted on 10 dumbbell-type samples of 5.0 mm ± 0.1 mm in thickness, gauge length of 24 mm ±

0.1 mm, and total length of 235 mm. The testing procedures followed the requirements of PN-EN ISO 527-3 (1998). Samples were subjected to a uni-axial tensile test on a Zwick 1445 testing machine (Zwick GmbH, Ulm, Germany) using a Dantec Dynamics system optical extensometer (Dantec Dynamics A/S, Skovlunde, Denmark). Table 1 presents the average properties of tested materials. The recorded properties are consistent with literature data for papers of comparable grammage (Szewczyk and Łapczyńska 2013). To date, no alternative results have been published for WoodEpox®. Uniaxial tensile tests made it possible to record directly the load, elongation, and narrowing of the samples. Based on this, the stress-strain relation was determined for each material, which was implemented for numerical calculations. This method was selected to be the most adequate way of material definitions in the finite element analysis. In further analysis the authors used the thickness of paper given above as a fixed value, and for the WoodEpox® due to technical processing limitations, the thickness of cell wall was t_A = 1.5 mm.

Table 1. Properties of Materials

MATERIAL	MOE_Y	MOE_X	MOR_Y	MOR_X	ϑ_{xy}	ϑ_{yx}
	[MPa]				-	
Paper	5142	1350	43	12.5	0.55	0.17
WoodEpox®	1029	-	5	-	0.3	

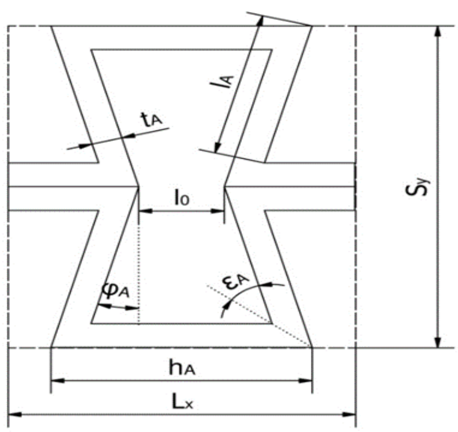

Fig. 1. Elementary core cell, where: t_A (mm): thickness of cell wall; l_A,h_A (mm): length of cell wall side, φ_A, ε_A(˚): interior angles of a cell; S_y, L_x (mm): overall dimensions of cell; l_0 (mm): distance between cell walls

Mathematical Models of Auxetic Cells

Analytical models of elastic constants for auxetic core cells are presented using geometry as in Fig. 1. Relative density ρ_A of the analyzed auxetic structure may be described as the product of core density ρ_A^* and density of the substance forming the skeleton of the structure ρ_{sA} (Eq. 1).

$$\rho_A = \frac{\rho_A^*}{\rho_{sA}}. \tag{1}$$

Following necessary transformations relative density may be written as follows:

$$\rho_A = \frac{F_{sA}}{F_A^*}. \tag{2}$$

The area of the elementary core section is represented by Eq. 3.

$$F_{\mathrm{A}}^{*} = 4\big(t_{\mathrm{A}} + l_{\mathrm{A}}cos(\varphi_{\mathrm{A}})\big)\big(h_{\mathrm{A}} - t_{\mathrm{A}}ctg(\varepsilon_{\mathrm{A}}) - l_{\mathrm{A}}sin(\varphi_{\mathrm{A}})\big). \qquad (3)$$

The area of the substance forming the skeleton of the structure may be described as follows:

$$F_{\mathrm{sA}} = 4\big(t_{\mathrm{A}} + l_{\mathrm{A}}cos(\varphi_{\mathrm{A}})\big)\big(h_{\mathrm{A}} - t_{\mathrm{A}}ctg(\varepsilon_{\mathrm{A}}) - l_{\mathrm{A}}sin(\varphi_{\mathrm{A}})\big) \\ -4l_{\mathrm{A}}cos(\varphi_{\mathrm{A}})\big(h_{\mathrm{A}} - 2\,t_{\mathrm{A}}ctg(\varepsilon_{\mathrm{A}}) - l_{\mathrm{A}}sin(\varphi_{\mathrm{A}})\big), \qquad (4)$$

Thus,

$$\rho_{\mathrm{A}} = 1 - \frac{l_{\mathrm{A}}cos(\varphi_{\mathrm{A}})(h_{\mathrm{A}} - 2\,t_{\mathrm{A}}ctg(\varepsilon_{\mathrm{A}}) - l_{\mathrm{A}}sin(\varphi_{\mathrm{A}})}{(t_{\mathrm{A}} + l_{\mathrm{A}}cos(\varphi_{\mathrm{A}}))(h_{\mathrm{A}} - t_{\mathrm{A}}ctg(\varepsilon_{\mathrm{A}}) - l_{\mathrm{A}}sin(\varphi_{\mathrm{A}}))}, \qquad (5)$$

where $\varepsilon_{\mathrm{A}} = \frac{90° - \varphi_{\mathrm{A}}}{2}$. (6)

The condition critical for the existence of an auxetic cell with the presented geometry is:

$$l_0 = 2\left(\frac{h_{\mathrm{A}}}{2} - l_{\mathrm{A}}sin(\varphi_{\mathrm{A}}) - t_{\mathrm{A}}ctg(\varepsilon_{\mathrm{A}})\right) > 0 \qquad (7)$$

and simultaneously:

$$90° > \varphi_{\mathrm{A}} > 0°. \qquad (8)$$

Elastic constants of cells presented below are given after Masters and Evans (1996). In this paper, modeled structures and materials were characterized by linear elasticity,

$$E_{\mathrm{y}} = \frac{K_{\mathrm{f}}(\frac{h_{\mathrm{A}}}{l_{\mathrm{A}}} + sin(\varphi_{\mathrm{A}}))}{Hcos^{3}(\varphi_{\mathrm{A}})}, \qquad (9)$$

$$E_{\mathrm{x}} = \frac{K_{\mathrm{f}}cos(\varphi_{\mathrm{A}})}{b\left(\frac{h_{\mathrm{A}}}{l_{\mathrm{A}}} + sin(\varphi_{\mathrm{A}})\right)\sin^{2}(\varphi_{\mathrm{A}})}, \qquad (10)$$

$$\upsilon_{\mathrm{xy}} = \frac{sin(\varphi_{\mathrm{A}})(\frac{h_{\mathrm{A}}}{l_{\mathrm{A}}} + sin(\varphi_{\mathrm{A}}))}{\cos^{2}(\varphi_{\mathrm{A}})}, \qquad (11)$$

$$\upsilon_{\mathrm{yx}} = \frac{\cos^{2}(\varphi_{\mathrm{A}})}{\left(\frac{h_{\mathrm{A}}}{l_{\mathrm{A}}} + sin(\varphi_{\mathrm{A}})\right)sin(\varphi_{\mathrm{A}})}, \qquad (12)$$

$$G_{\mathrm{xy}} = \frac{K_{\mathrm{f}}(\frac{h_{\mathrm{A}}}{l_{\mathrm{A}}} + sin(\varphi_{\mathrm{A}}))}{H\left(\frac{h_{\mathrm{A}}}{l_{\mathrm{A}}}\right)^{2}\left(1 + \frac{2h_{\mathrm{A}}}{l_{\mathrm{A}}}\right)cos(\varphi_{\mathrm{A}})}. \qquad (13)$$

where E_{x} (MPa) is Young's modulus in the X axis, E_{y} (MPa) is Young's modulus in the Y axis, ϑ_{xy} is Poisson's ratio in plane XY, ϑ_{yx} is Poisson's ratio in plane YX, G_{xy} (MPa) is the modulus of elasticity in shear, $K_f = \frac{E_s H t_{\mathrm{A}}^{3}}{l_{\mathrm{A}}^{3}}$ (N/m) is the bending force constant, and E_{s} (MPa) is Young's modulus of the core substance.

Monte Carlo Optimization

In engineering computations, statistical methods constituting a component of numerical methods are used in static optimization (Smardzewski 2015). In this study, the cell shape was optimized using the Monte Carlo approach, consisting of random searches for the admissible area and on the basis of results to estimate the optimal value. In this case the maximization of the moduli of elasticity, E_x (MPa) and E_y (MPa), for the developed core cells was considered to be a natural optimization criterion. The set of decision variables comprised outer dimensions of cells, dimensions, and angles of cell walls. The optimal solution may be reached after a conjunctive satisfaction of numerous limiting conditions, resulting from cell shape. A significant limiting criterion was connected with the specific density of a hexagonal cell, most frequently found in honeycomb panels used in the furniture industry ($\rho_A = 0.0249$). The mathematical model for the optimization of a polygonal auxetic cell included the following,

a) decision variables, for which the variables block K_z takes the form in Eq. 14,

$$K_z = \left\{\bar{x} = (x_1 \dots x_4)\colon x_{i(\min)} \le x_i \le x_{i(\max)}\colon i = 1 \dots 4\right\} \tag{14}$$

where i is the number of decision variables for the cell, $x_1 = t_A$ (mm) cell wall thickness, $x_2 = h_A$ (mm) length of a common cell wall, $x_3 = l_A$ (mm) length of a free cell wall, and $x_4 = f_A$ (°) is the angle of a cell wall,

b) parameter E_s (MPa) Young's modulus of the material, from which cell walls were manufactured,

c) admissible set Φ was produced from inequality restrictions $\Phi_i(x) > 0$, *i.e.*:

$$\Phi = \{\bar{x} = (x_1 \dots x_4)\colon \Phi_i(\bar{x}) > 0\colon i = 1 \dots 4\} \tag{15}$$

The critical condition for the existence of an auxetic cell with the presented geometry was as follows:

$$l_0 > 0 \text{ (mm)} \tag{16}$$

The objective function as maximization of values for Young's moduli of a cell in the primary orthotropic directions was as follows.

$$f(opt.) = E_x \rightarrow max \text{ and } E_y \rightarrow max. \tag{17}$$

The optimization program was written in the Visual Basic programming language (Microsoft, Redmond, WA, USA). A total of 30000 samplings were performed, among which approx. 0.03% were successful. Table 2 presents values of elastic constants calculated based on formulas 9 through 13 for optimized cells. In turn, Fig. 2 presents shapes of cells selected through optimization. Cells A through D are characterized by relative density identical in relation to the reference cell $\rho_A = 0.0249$. The shape of cell E made from WoodEpox® is the result of maintaining technical feasibility of the core at the maximum values of Young's moduli and minimum relative density $\rho_A = 0.1547$. Moreover, it results from Table 2 that cell D exhibits considerable orthotropy: a high value of Young's modulus in the direction of the Y axis, as well as a low value of Poisson's ratio ϑ_{yx}. Greater values of elastic properties in comparison to paper cells are recorded for cell E. This is caused by a significant increase in cell wall thickness at a comparable scale of overall dimensions of the cell. Cells A through C were at comparable dimensions, L_x and S_y differ significantly in the cell wall angle. Selected cells were used in further modeling.

Table 2. Elastic Properties Provided by Mathematical Analysis

Cell type	E_x	E_y	ϑ_{xy}	ϑ_{yx}
	[MPa]		-	
A	0.033	0.194	-0.42	-2.40
B	0.023	0.458	-0.23	-4.43
C	0.033	0.058	-0.75	-1.32
D	0.0001	1.109	-0.03	-38.0
E	2.049	47.906	-0.21	-4.83

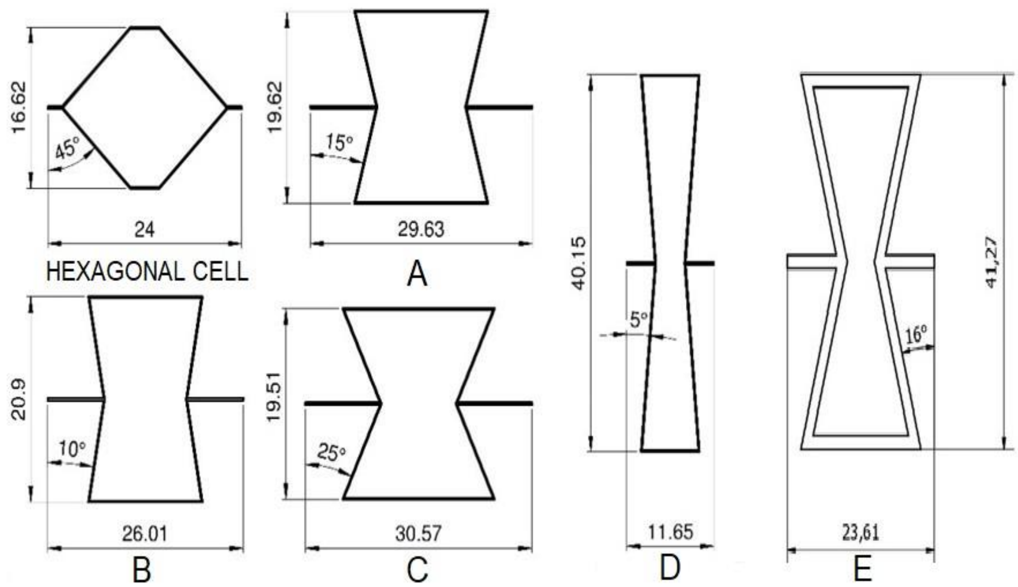

Fig. 2. Elementary core cells: Hexagonal cell, the reference cell with relative density ρ_A = 0.0249; A through D: paper cells; E: WoodEpox® cell

As shown, the inclination angle φ_A differed within range 1 to 25°, cell length l_A, h_A respectively within range 5 to 20 mm. The relative density of the paper cells was a fixed value ρ_A = 0.0249, whereas relative density of the WoodEpox® ρ_A = 0.1547.

Numerical Models

Numerical computations were performed using the Finite Element Method (FEM) applying the Abaqus v6.13 program (Dassault Systemes Simulia Corp., Waltham, MA, USA) and the resources of the EAGLE computational cluster, the Poznań Supercomputing and Networking Center, within the framework of the computational grant, "Properties of furniture panels with the synclastic surface and an auxetic core". The computational model is presented in Fig. 3. The HEX (hexahedral elements) grid was applied along with elastic-plastic strains for selected materials (Table 1). The models were characterized by the mean number of nodes ranging from 0.6 million to 1.4 million and the mean number of elements ranging from 0.4 million to 1.2 million. The C3D6 (wedge) and C3D8R (tetrahedral) solid elements were used.

Calculations were made for loads in the direction of the X axis, and next in the Y axis for recording respective strains. For the paper models, variable loads were assumed ranging from 0 N to 0.1 N at an increment of 0.02 N for the direction of the X axis and from 0 N to 0.3 N at an increment of 0.05 N for the direction of the Y axis. For the

WoodEpox ® model it was from 0 N to 10 N at an increment of 2 N and from 0 N to 35 N at an increment of 5 N. Results of calculations are given in Table 3.

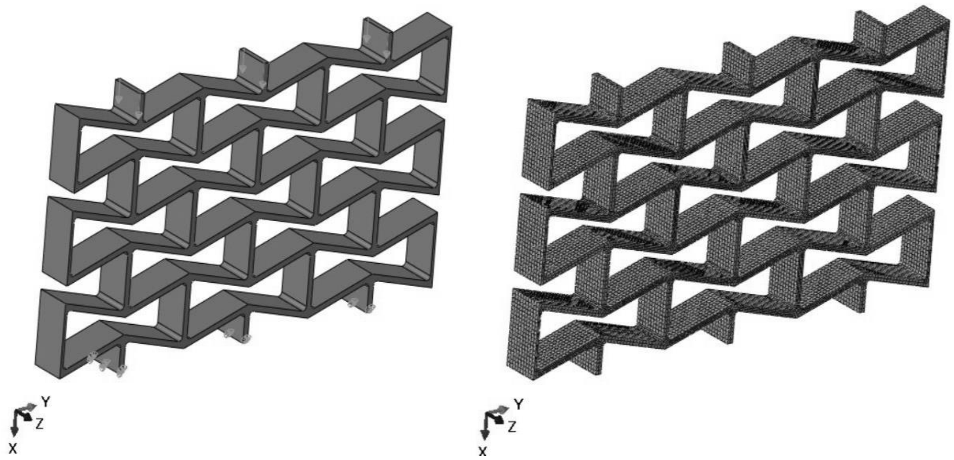

Fig. 3. An example model of a core used in numerical computations; Left is a diagram of loads, and right is a mesh grid for the model

Table 3. Elastic Properties Provided by FEM

Cell type	E_x	E_y	ϑ_{xy}	ϑ_{yx}
	[MPa]		-	
A	0.0148	0.0224	-0.7056	-0.8645
B	0.0167	0.0393	-0.7777	-1.0227
C	0.0116	0.0198	-0.7760	-0.7393
D	0.0076	0.0875	-0.3465	-2.5368
E	0.1467	4.9693	-0.1774	-5.2667

As shown in Table 3, cores showed negative Poisson's ratios. The highest Young's moduli, E_y = 4.97 MPa and E_x = 0.15 MPa, were found for the core with cell E. It also showed the lowest value of Poisson's ratio, ϑ_{yx} = -5.23. Among the cores with paper cells, the highest value of the modulus, E_y = 0.0875 MPa, was found for the core with cell D. At the same time, it is a model with the greatest orthotropy, since the modulus of elasticity in the direction was E_x = 0.0076 MPa. The core with cell D also showed a low value of Poisson's ratio ϑ_{yx} = -2.54, while ϑ_{xy} = -0.35. Cores with cells A through C are characterized with evident orthotropy of elastic properties. In the case of C type cells, the values of Young's moduli and Poisson's ratios were very similar. This results in the core with mechanical properties close to the isotropic structure. Furthermore, a smaller angle in the wall led to a greater increase in Young's modulus E_y (MPa), while the difference between Poisson's ratios ϑ_{xy} and ϑ_{yx} increased as well.

Experimental Tests

In the next stage of the study, molds facilitating technical manufacture of paper cores were designed. These molds in the form of 3D solids (Fig. 4.) were designed in the Autodesk Inventor Professional® environment (Autodesk, San Rafael, CA, USA) and finished models were exported to the STL format. They were printed on a Stratasys Fortus 400mc small printer (Stratasys, Eden Prairie, MN, USA) using FDM Nylon-12™ filament (Stratasys, Minnesota, USA).

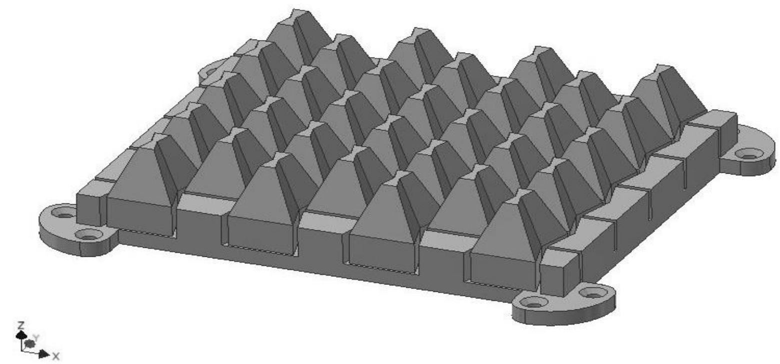

Fig. 4. An example mold to manufacture the selected paper core

Sheets of paper were embossed and cut into strips of 10 mm in width using a Kongsberg-X plotter (Esko, Ghent, Belgium). The next step was to glue single strips into sets using the PVAC Woodmax FF 12.47 D2 adhesive (Synthos, Oświęcim, Poland). Such prepared sets were pulled onto the mold. The core shape was fixed using a SLW 15 laboratory dryer (Pol-Eko-Aparatura, Warsaw, Poland) at a temperature of 180 ± 1°C for 300 s. In case of the WoodEpox®, panels of 10 ± 0.2 mm in thickness were manufactured. Panels were sanded on a Felder FW 1102 perform wide belt sander (Felder Group, Żory, Poland) and milled on a Kongsberg-X milling cutter using an HM straight shank cutter of 3 mm in diameter (CMT, Poznań, Poland). Five cores each were manufactured to determine properties in planes XY and YX. Figure 5 presents the manufactured cores.

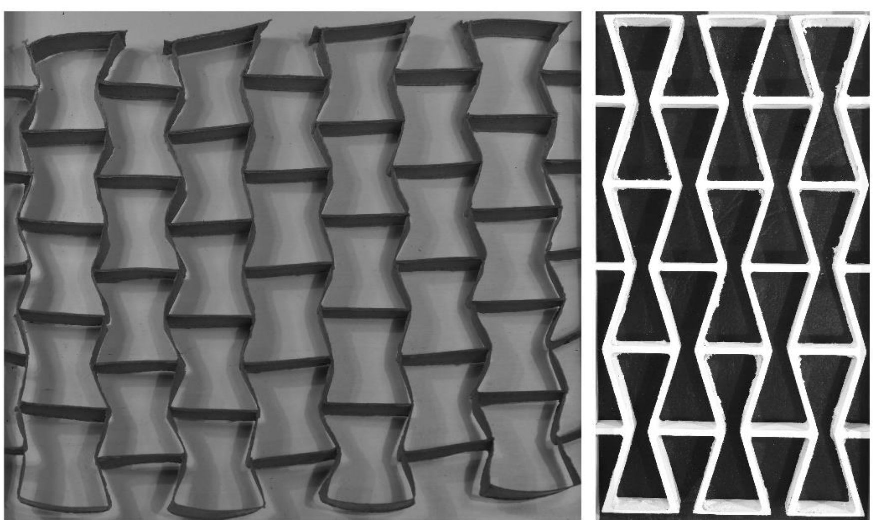

a) **b)**

Fig. 5. a) Example paper core type D, b) core E manufactured from WoodEpox®

Cores were subjected to uniaxial compression (Fig. 6). The testing stand was composed of a support beam, on which the sample and platens were placed. A ZEMIC H3-C3-25kg-3B sensor (Serial No. P2Z122353) (Zemic, Hanzhong, China) was placed between the platens, recording the force exerted onto the tested element accurate to 0.001 N. The stand was lighted with two lamps of 630 lumens to ensure proper photographic recording of the test.

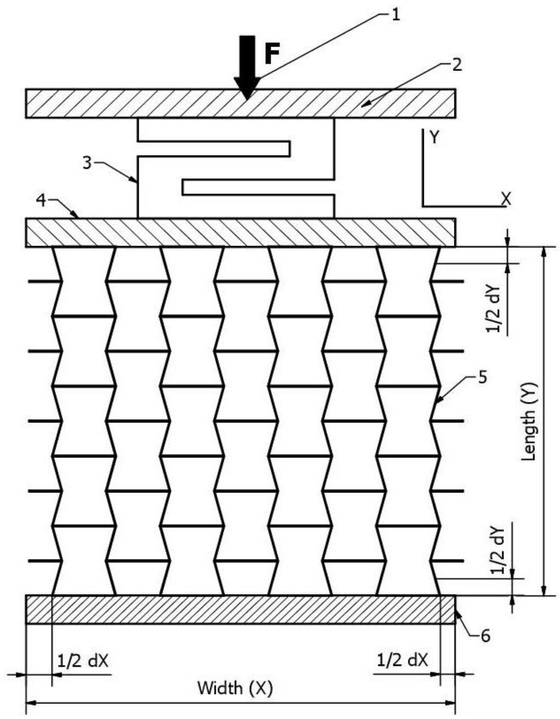

Fig. 6. The testing stand: 1) pressing screw, 2) sensor platten, 3) ZEMIC H3-C3-25kg-3B sensor, 4) sample platten, 5) tested sample, and 6) support

Samples were tested following the analogical method, which was applied in numerical calculations. For each applied load a monochromatic image was taken using an Olympus OM-D camera (Olympus, Tokyo, Japan). Next strains were measured in the core by analyzing the images using the National Instruments IMAQ Vision Builder 6.1 linear analysis software (National Instruments, Austin, TX, USA) (Fig. 7).

The edge detection method was applied in digital image analysis, and respective Poisson's ratios and Young's moduli were calculated from the dependence shown below,

$$\vartheta_{yx} = \frac{dX \cdot Y}{X \cdot dY} \text{ for loading direction Y} \tag{18}$$

$$\vartheta_{xy} = \frac{dY \cdot X}{Y \cdot dX} \text{ for loading direction X} \tag{19}$$

where dX (mm) and dY (mm) are displacements in directions X and Y, X (mm) is width, Y (mm) is length of the core,

$$E_y = \frac{Fy \cdot Y}{H \cdot X \cdot dY} \text{ for loading direction Y} \tag{20}$$

$$E_x = \frac{Fx \cdot X}{H \cdot Y \cdot dX} \text{ for loading direction X} \tag{21}$$

where $F_{x,y}$ (N) are loads for directions X and Y, H (mm) is height of the core, dX (mm) and dY (mm) are displacements in directions X and Y, respectively.

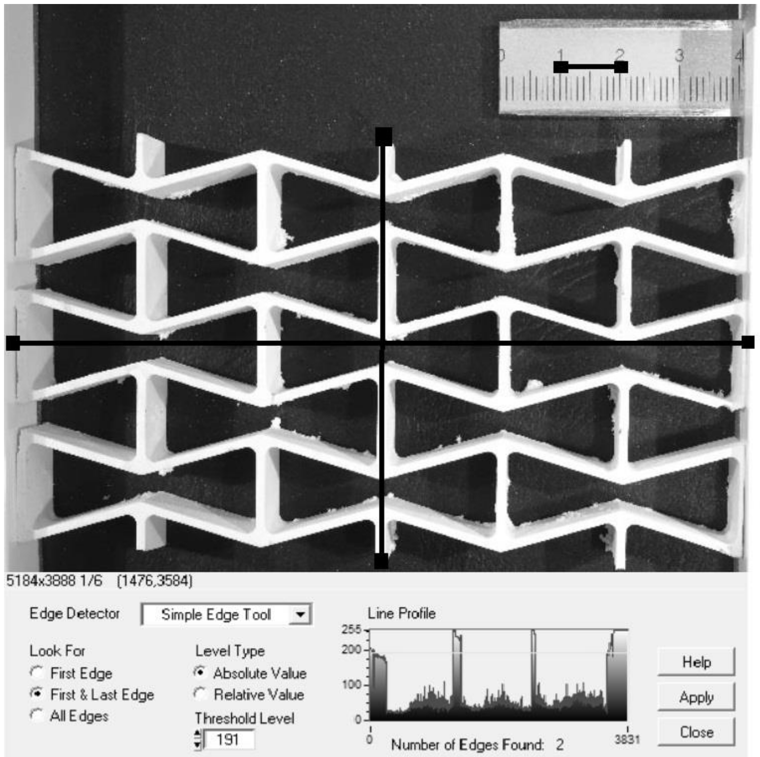

Fig. 7. The method to measure strain: detection of gauge points

Based on the image analysis elastic constants of the tested cores were determined, as presented in Table 4.

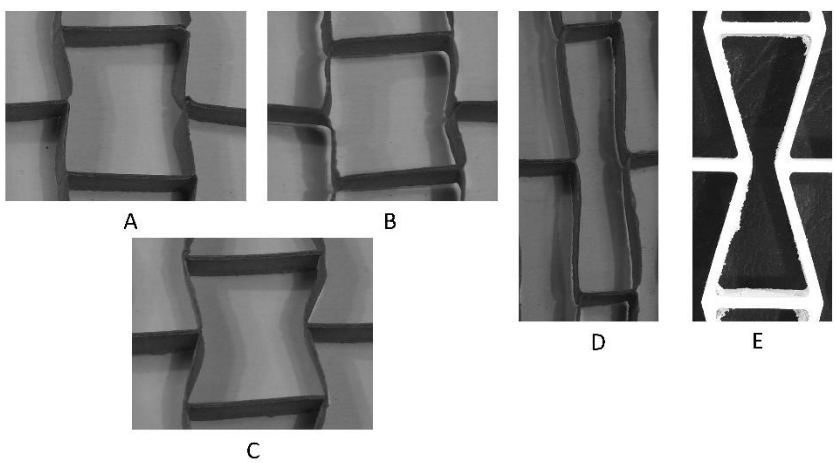

Fig. 8. Images of elementary cells in cores: A through D: paper cores; E: WoodEpox® core

During the paper expanding process, the cells of the core are expanding differently. The width of the adhesive stream is not repeatable, which has a significant impact on the length of the free and common cell wall. This affects the inclination angles as shown in Fig. 9. Measured angles of inclination differ from each other, $\varphi_{A1} \neq \varphi_{A2} \neq \varphi_{A3} \neq \varphi_{A4}$.

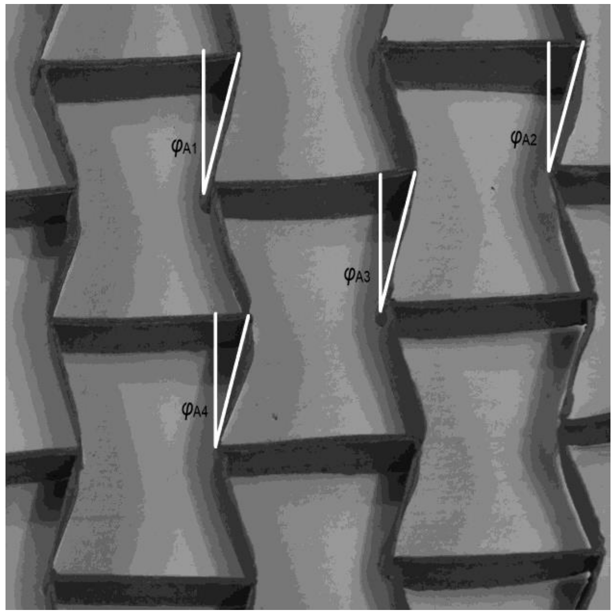

Fig. 9. Different angles of inclination of tested core D fragment

Scanned images of real cores allowed to remodel cores for finite element method. With the analytical approach, real cell geometric dimensions were used to recalculate the elastic properties, with no further corrections to the cell geometry.

Table 4. Elastic Properties of the Core from the Experimental Sample

	E_x	E_y	ϑ_{xy}	ϑ_{yx}
Cell type	[MPa]		-	
A	0.0148	0.0227	-0.7092	-0.8522
B	0.0195	0.0413	-0.9842	-1.0446
C	0.0114	0.0213	-0.7072	-0.7222
D	0.0083	0.0915	-0.3049	-2.7411
E	0.1201	5.4655	-0.1915	-5.9104

Table 4 shows that the greatest values of Young's modulus, E_y = 5.47 MPa and E_x = 0.12 MPa, were recorded for the core with the E type cells. This core was also characterized by the lowest Poisson's ratio ϑ_{yx} = -5.91, while ϑ_{xy} = -0.19. Among paper cores, the greatest value of the modulus E_y = 0.0915 MPa was recorded for the core with the D type cells, with E_x = 0.0083 MPa. During tests of this core, it was also most prone to buckling due to its slenderness. Among cores manufactured from paper, it showed a low value of Poisson's ratio by ϑ_{yx} = -2.74 and ϑ_{xy} = -0.30. When analyzing properties of cores with cell types A through C it needs to be stressed that similar to the previous ones, they exhibited orthotropic properties. Only the core with type C cells showed comparable values of ϑ_{xy} and ϑ_{yx} and slightly varied values of moduli E_x = 0.0213 MPa, E_y = 0.0114 MPa.

RESULTS AND DISCUSSION

Digital image analysis for the geometry of elementary core cells was used to determine their actual dimensions with imperfections. Table 5 presents major parameters of geometry for actual cells and idealized (theoretical) cells. The main imperfections in geometry are caused by changes in linear dimensions of wall length and angles, while in the case of paper cores, it was also wall shape. Core type E exhibited the smallest differences in dimensions, as it has the most accurate manufacturing technology. Changes in geometry resulted from the uneven structure of the material and technological feasibility of its manufacture. Dimensions of cells with imperfections were used in the repeated mathematical modeling of elastic properties of the core using equations 8 through 12. Figure 10 presents a comparison of values for Young's moduli E_{x} (MPa), E_{y} (MPa) of theoretical cells A, B, C, D, and E, as well as Young's moduli $E_{\mathrm{x}}^{\mathrm{R}}$ (MPa), $E_{\mathrm{y}}^{\mathrm{R}}$ (MPa) of analogous actual cells. In turn, Fig. 11 presents a comparison of Poisson's ratios ϑ_{xy}, ϑ_{yx} of theoretical cells A, B, C, D, and E, as well as Poisson's ratios $\vartheta_{\mathrm{xy}}^{\mathrm{R}}$, $\vartheta_{\mathrm{yx}}^{\mathrm{R}}$ of analogous actual cells.

Table 5. Dimensions of Actual (R) and Theoretical Cells (T)

Cell Dimension	A		B		C		D		E	
	R	T	R	T	R	T	R	T	R	T
l_A [mm]	19.96	17.403	16.23	14.821	19.86	19.746	8.04	7.568	19.15	19.290
h_A [mm]	9.64	10.010	9.46	10.460	9.46	10.598	17.97	20.001	19.31	20.685
φ_A [°]	-13.9	-15	-8.9	-10	-22.3	-25	-6.4	-5	-16.4	-16
H [mm]	9.99	10	10.03	10	10.00	10	10.01	10	10.04	10

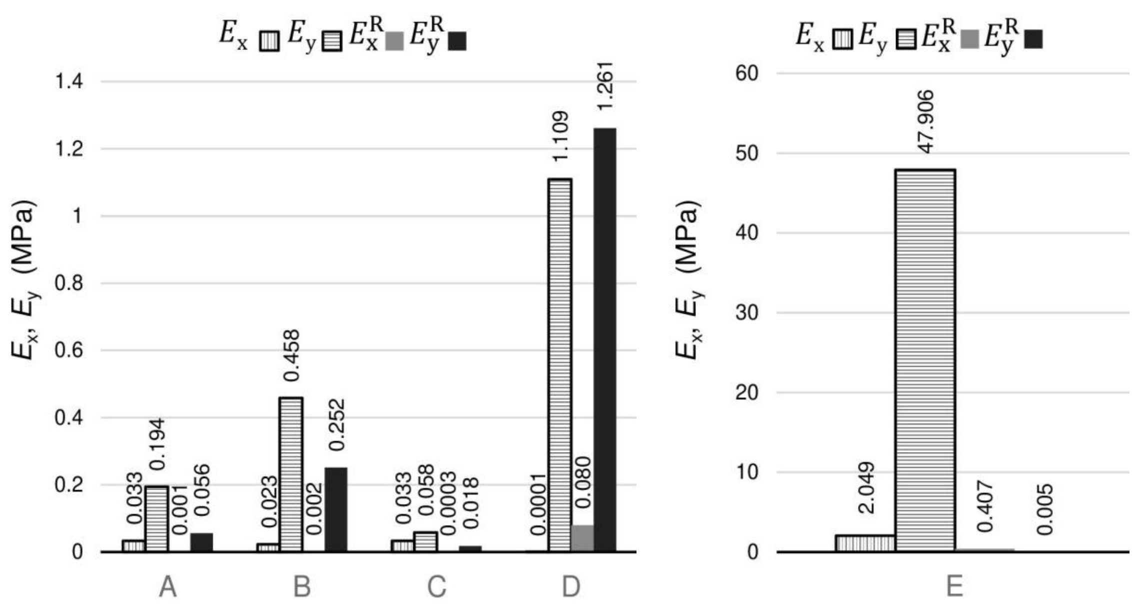

Fig. 10. Analytical values of Young's moduli for theoretical and actual models

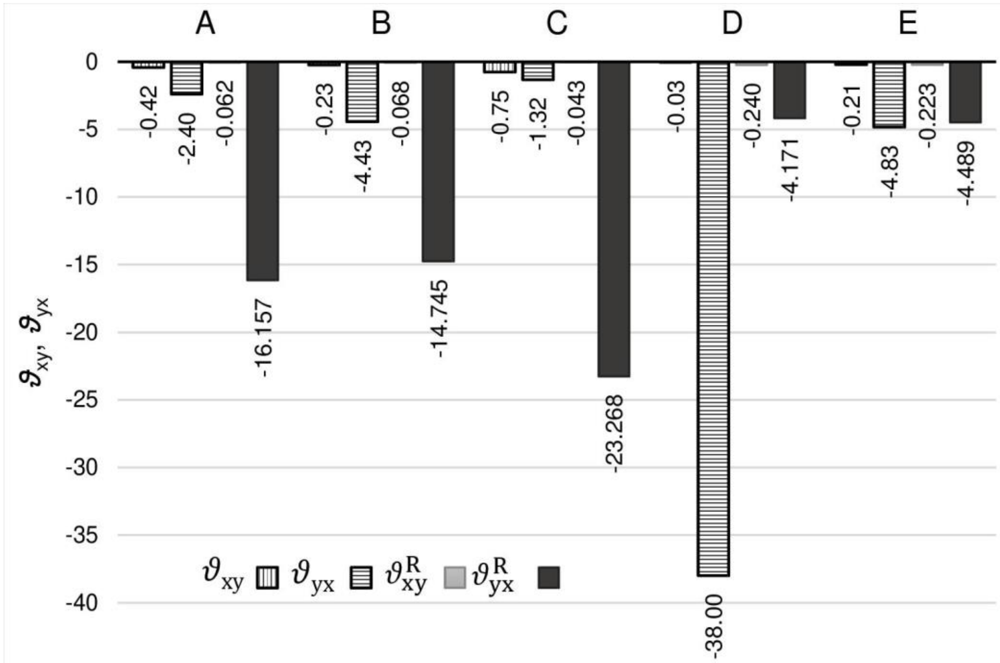

Fig. 11. Analytical values of Poisson's ratio for theoretical and actual models

As shown in Figs. 10 and 11, cell geometry strongly affects its elastic properties. A particularly important role is played by the effect of the cell wall angle f_A, while as a result of the manufacturing technology of paper cores it is susceptible to changes. For paper cores with cells A through C, the obtained interior angles of cells were much more obtuse than theoretically assumed, while for cell D the angle was less obtuse than it had been assumed. For cell E, no marked change was observed in Poisson's ratio (6% to 7%). However, Young's modulus E^{R}_{x} (MPa) of that cell decreased 400-fold in relation to the idealized models E_x (MPa) , while in the case of modulus E^{R}_{y} (MPa) it was over 100-fold. The greatest changes in values of Poisson's ratio were observed for type C cells. In that case the index ϑ^{R}_{yx} of the physical model increased over 17-fold in relation to the idealized model ϑ_{yx}. This was caused by a change in angle f_A of the cell wall. For cells A and B, the change in Poisson's ratio was much smaller. In the case of cell A, an almost 7-fold increase in ϑ^{R}_{yx} compared to ϑ_{yx} was observed, while in the case of cell B it was almost 3-fold. In turn, for cell D the value of ϑ^{R}_{yx} decreased 9-fold in relation to ϑ_{yx}. Analogously, for cells A through C values of ϑ^{R}_{xy} decreased in relation to ϑ_{xy}. Values of Young's moduli E_x (MPa) for cells A through C turned out to be as much as 11-fold greater in relation to E^{R}_{x} (MPa). Cell D exhibited strong orthotropy, and the respective differences exceeded 800%. For cells A through C, values of E_y (MPa) were 2- to 4-fold greater in comparison to the results of mathematical analysis based on actual dimensions.

Figure 12 compares Young's moduli E_x (MPa), E_y (MPa) for cells A, B, C, D, and E that was established based on numerical calculations (FEM) and experimental tests (EXP), while Fig. 13 gives analogous values of Poisson's ratio ϑ_{xy}, ϑ_{yx}.

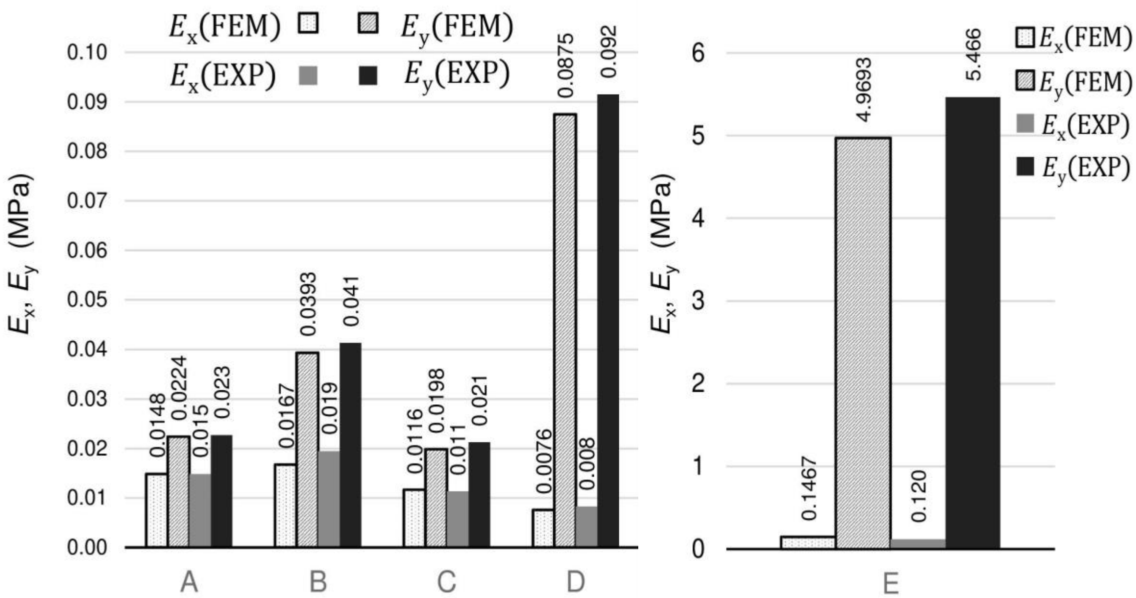

Fig. 12. Young's moduli E_x, E_y determined numerically and experimentally

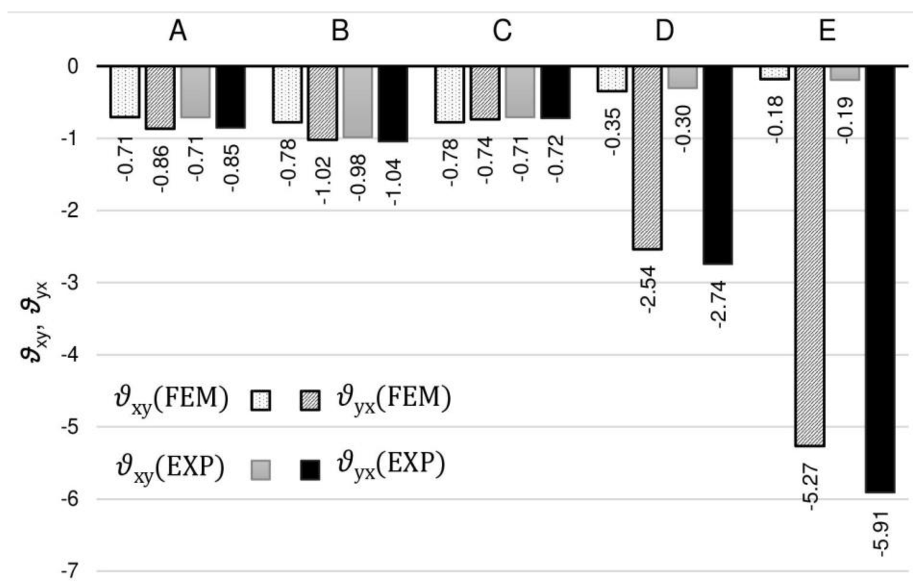

Fig. 13. Poisson's ratios determined numerically and experimentally

When comparing results of FEM analyses and experimental tests of paper cores, the greatest differences were recorded for modulus E_x (MPa) of type B core. The result of numerical simulations was by 14% lower than that obtained in experimental tests. In turn, for calculations of modulus E_y (MPa), a considerable difference was recorded for type C core. In that case the results were by 7% lower than the value of the laboratory measurement. For the WoodEpox® core, numerical analysis made it possible to estimate the modulus E_x (MPa) with a value by 22% lower in comparison to the experimental results. In turn, the value of modulus E_y (MPa) was by approx. 9% lower. The other results of numerical calculations for paper cores in comparison to the experimental results differed by max. 9%. This may be considered a satisfactory agreement. When analyzing the quality of calculations for Poisson's ratio the greatest difference in relation to laboratory tests was found for Poisson's ratio ϑ_{xy} for core B. Obtained values were by approx. 21% lower in comparison to those recorded in the experiment. For type D core the value of ϑ_{yx} was by 8% lower in relation to the experimental results, while for core E values from numerical simulations of ϑ_{xy} and ϑ_{yx} were by 8% to11% lower. For the other cell types the differences in values of Poisson's ratios were calculated numerically in relation to the results recorded in the experiment and they did not exceed 13%. This may also be considered a satisfactory consistency with the experimental findings resulting from an accurate representation of geometry and material properties in numerical models.

In turn, evident and marked differences were found between the results of experimental tests and analytical calculations. The mathematical simulation shows significant sensitivity to imperfections of cell geometry. When considering the idealized mathematical model, free from imperfections, the results of calculations for paper cores are much lower than the recorded experimental results. Differences exceeded several fold between the results of the laboratory tests. The greatest difference, over 30-fold, was recorded for the simulation of Poisson's ratio ϑ_{yx} for the core with type C cells. In turn, smaller, although still considerable differences were recorded for the simulation of elastic properties of type E core. Although the simulation of values of Young's moduli E_x (MPa) and E_y (MPa) is far from satisfactory, it needs to be stressed that Poisson's ratio was determined with a 16% to 25% difference in values. This results from a highly precise processing of core E and its shape being almost identical to that assumed analytically.

As indicated above, there were significant differences between experimental research and analytical modeling. Taking into consideration the proximity of the FEM analysis to the experiment, in most cases not exceeding 9% of the error, it should be noted that there was no unambiguous tendency for the results to overestimate or underestimate with use of the FEM analysis. Therefore, it should be pointed out that the results obtained from the FEM analysis are also significantly different from the analytical approach - several to several hundred times.

CONCLUSIONS

1. Cell geometry has a considerable effect on elastic properties of cell cores. The change in the cell wall angle is particularly significant.
2. The WoodEpox® biocomposite is a suitable material for the manufacture of light layered composites because the imperfections were slight enough.
3. Geometrical imperfections of paper cores have a considerable effect on the results of analytical calculations. Idealized analytical models indicate very large differences in comparison to experimental tests or numerical simulations.
4. Implementation of geometrical imperfections in modeling of CAD models used for FEM method, shows that results differ significantly from analytical approach.
5. Based on numerical calculations a satisfactory consistency of the results was obtained in relation to the data from experimental tests. This similarity is a result of the representation of geometrical imperfections in numerical modeling.
6. Investigated cores show orthotropic properties, which justifies their application in semi-finished elements or elements with a highly precise character of loads.

ACKNOWLEDGMENTS

Calculations were conducted using the computational resources of the EAGLE computational cluster, of the Poznań Supercomputing and Networking Center, within the framework of the computational grant, "Properties of furniture panels with the synclastic surface and an auxetic core".

The present work was conducted as part of a research project (No. 2016/21/B/ST8/01016) financed from the funds of the National Science Centre.

REFERENCES CITED

Gay, D., Hoa, S., and Tsai, S. (2003). *Composite Materials: Design and Applications*, CRC Press, Boca Raton, FL, USA. DOI: 10.1201/9781420031683

Geers, M. G. D., Kouznetsova, V. G., and Brekelmans, W. A. M. (2010). "Multi-scale computational homogenization: Trends and challenges," *Journal of Computational and Applied Mathematics* 234(7), 2175-2182. DOI: 10.1016/j.cam.2009.08.077

Guedes, J., and Kikuchi, N. (1990). "Preprocessing and postprocessing for materials based on the homogenization method with adaptive finite element methods," *Computer Methods in Applied Mechanics and Engineering* 83(2), 143-198. DOI: 10.1016/0045-7825(90)90148-f

Hartung, D., Sickinger, C., and Herbeck, L. (2003). "A simple homogenization method for a flat periodic plate structure," in: *Proceedings Second MIT Conference on Computational Fluid and Solid Mechanics*, Boston, pp. 2294-2297. DOI: 10.1016/b978-008044046-0.50563-7

Herup, E. J., and Palazotto, A. N. (1998). "Low-velocity impact damage initiation in graphite/epoxy/Nomex honeycomb-sandwich plates," *Composites Science and Technology* 57(12), 1581-1598. DOI: 10.1016/S0266-3538(97)00089-4

Hohe, J., and Becker, W. (2001). "Effective stress-strain relations for two-dimensional cellular sandwich cores: Homogenization, material models, and properties," *Applied Mechanics Reviews* 55(1), 61-87. DOI: 10.1115/1.1425394

Imbalzano, G., Linforth, S., Ngo, T. D., Lee, P. V. S., and Tran, P. (2018). "Blast resistance of auxetic and honeycomb sandwich panels: Comparisons and parametric designs," *Composite Structures* 183(1), 242-261. DOI: 10.1016/j.compstruct.2017.03.018

Imbalzano, G., Tran, P., Ngo, T. D., and Lee, P. V. (2017). "Three-dimensional modelling of auxetic sandwich panels for localised impact resistance," *Journal of Sandwich Structures & Materials* 19(3), 291-316. DOI: 10.1177/1099636215618539

Jeong, S., Zhu, F., Lim, H., Kim, Y., and Yun, G. J. (2019). "3D stochastic computational homogenization model for carbon fiber reinforced CNT/epoxy composites with spatially random properties," *Composite Structures* 207, 858-870. DOI: 10.1016/j.compstruct.2018.09.025

Majewski, A., and Smardzewski, J. (2015). "Models for elastic deformation of auxetic honeycomb with triangular cells," in: *Proceedings of the XXVIIth International Conference Research for Furniture Industry*, Ankara, Turkey, pp. 256-268.

Masters, I. G., and Evans, K. E. (1996). "Models for the elastic deformation of honeycombs," *Composite Structures* 35(4), 403-422. DOI: 10.1016/S0263-8223(96)00054-2

Mousanezhad, D., Haghpanah, B., Ghosh, R., Hamouda, A. M., Nayeb-Hashemi, H., and Vaziri, A. (2016). "Elastic properties of chiral, anti-chiral, and hierarchical honeycombs: A simple energy-based approach," *Theoretical and Applied Mechanics Letters* 6(2), 81-96. DOI: 10.1016/j.taml.2016.02.004

Nilsson, E., and Nilsson, A. C. (2002). "Prediction and measurement of some dynamic properties of sandwich structures with honeycomb and foam cores," *Journal of Sound and Vibration* 251(3), 409-430. DOI: 10.1006/jsvi.2001.4007

Paik, J. K., Thayamballi, A. K., and Kim, G. S. (1999). "The strength characteristics of aluminum honeycomb sandwich panels," *Thin-Walled Structures* 35(3), 205-231. DOI: 10.1016/S0263-8231(99)00026-9

Pan, S. -D., Wu, L. -Z., and Sun, Y.-G. (2008). "Transverse shear modulus and strength of honeycomb cores," *Composite Structures* 84(4), 369-374. DOI: 10.1016/j.compstruct.2007.10.008

Park, K. -J., Jung, K., and Kim, Y.-W. (2016). "Evaluation of homogenized effective properties for corrugated composite panels," *Composite Structures* 140, 644-654. DOI: 10.1016/j.compstruct.2016.01.002

PN-EN ISO 1924-2 (2010). "Papier i tektura -- Oznaczanie właściwości przy działaniu sił rozciągających -- Część 2: Badanie przy stałej prędkości rozciągania (20 mm/min) [Paper and cardboard - Determination of tensile properties - Part 2: Test at constant tensile speed (20 mm / min)]," Polish Committee for Standardization, Poland.

PN-EN ISO 527-3 (1998). "Tworzywa sztuczne -- Oznaczanie właściwości mechanicznych przy statycznym rozciąganiu -- Warunki badań folii i płyt [Plastics - Determination of mechanical properties at static tension - Test conditions for films and plates]," Polish Committee for Standardization, Poland.

Pozniak, A. A., and Wojciechowski, K. W. (2014). "Poisson's ratio of rectangular anti-chiral structures with size dispersion of circular nodes," *Physica Status Solidi (b)* 251(2), 367-374. DOI: 10.1002/pssb.201384256

Rejab, M. R. M., and Cantwell, W. J. (2013). "The mechanical behaviour of corrugated-core sandwich panels," *Composites Part B: Engineering* 47, 267-277. DOI: 10.1016/j.compositesb.2012.10.031

Smardzewski, J. (2013). "Elastic properties of cellular wood panels with hexagonal and auxetic cores," *Holzforschung* 67(1), 87-92. DOI: 10.1515/hf-2012-0055

Smardzewski, J. (2015). *Furniture Design*, Springer International Publishing, New York, USA. DOI: 10.1007/978-3-319-19533-9

Smardzewski, J., and Majewski, A. (2014). "Mechanical properties of auxetic honeycomb core with triangular cells," in: *25th International Scientific Conference: New Materials and Technologies in the Function of Wooden Products*, Zagreb, Croatia, pp. 103-112.

Szewczyk, W., and Łapczyńska, M. (2013). "Changes of paper and paper products strength under long-lasting load," *Przegląd Papierniczy* 69, Prace Naukowo-Badawcze 378, 377-382.

Wadley, H. N. G., Dharmasena, K. P., O'Masta, M. R., and Wetzel, J. J. (2013). "Impact response of aluminum corrugated core sandwich panels," *International Journal of Impact Engineering* 62, 114-128. DOI: 10.1016/j.ijimpeng.2013.06.005

Wadley, H. N. G., Fleck, N. A., and Evans, A. G. (2003). "Fabrication and structural performance of periodic cellular metal sandwich structures," *Composites Science and Technology* 63(16), 2331-2343. DOI: 10.1016/S0266-3538(03)00266-5

Wang, B., Hu, J., Li, Y., Yao, Y., Wang, S., and Ma, L. (2018). "Mechanical properties and failure behavior of the sandwich structures with carbon fiber-reinforced X-type lattice truss core," *Composite Structures* 185, 619-633. DOI: 10.1016/j.compstruct.2017.11.066

Wang, B., Zhang, G., He, Q., Ma, L., Wu, L., and Feng, J. (2014). "Mechanical behavior of carbon fiber reinforced polymer composite sandwich panels with 2-D lattice truss cores," *Materials & Design* 55, 591-596. DOI: 10.1016/j.matdes.2013.10.025

Wang, X.-T., Wang, B., Li, X.-W., and Ma, L. (2017). "Mechanical properties of 3D re-entrant auxetic cellular structures," *International Journal of Mechanical Sciences* 131-132, 396-407. DOI: 10.1016/j.ijmecsci.2017.05.048

Wu, Q., Ma, L., Gao, Y., and Xiong, J. (2017). "A new fabrication method for hierarchical truss materials with millimeter-scale struts," *Materials Letters* 186, 1-6. DOI: 10.1016/j.matlet.2016.09.024

Xue, Z., and Hutchinson, J. W. (2006). "Crush dynamics of square honeycomb sandwich cores," *International Journal for Numerical Methods in Engineering* 65(13), 2221-2245. DOI: 10.1002/nme.1535

Yang, L., Harrysson, O., West, H., and Cormier, D. (2015). "Mechanical properties of 3D re-entrant honeycomb auxetic structures realized via additive manufacturing," *International Journal of Solids and Structures* 69-70, 475-490. DOI: 10.1016/j.ijsolstr.2015.05.005

Article submitted: November 22, 2018; Peer review completed: February 3, 2019; Revised version received: February 14, 2019; Accepted: February 16, 2019; Published: February 25, 2019.
DOI: 10.15376/biores.14.2.2977-2994